



Cyclic behavior of shear-and-flexural yielding metallic dampers



Dipti Ranjan Sahoo*, Tarun Singhal, Satpal Singh Taraitia, Ajay Saini

Department of Civil Engineering, Indian Institute of Technology Delhi, New Delhi, 110016, India

ARTICLE INFO

Article history:

Received 26 May 2014
Received in revised form 12 June 2015
Accepted 3 August 2015
Available online xxxx

Keywords:

Cyclic behavior
Experiments
Finite element analysis
Metallic devices
Shear links
Yielding

ABSTRACT

The energy dissipation potential of a metallic damper largely depends on the hysteretic response achieved due to the inelastic deformation of plates under either axial or flexural or shear loading. In this study, a passive energy dissipation device consisting of a series of steel plates capable of yielding in both flexure and shear has been experimentally investigated under cyclic loading. Two end plates of X-configuration are allowed to yield under flexural action, whereas a rectangular web plate of the device is allowed to dissipate energy through shear yielding. Three shear-and-flexural yielding damping (SAFYD) devices are studied by varying the size of both flexure and shear plates. The main parameters investigated are load-carrying capacity, hysteretic response, energy dissipation, equivalent viscous damping, and ductility. A finite element analysis has been carried out to predict the ultimate resistance and hysteretic response of the test specimen. The predicted results matched reasonably well with the test results. Finally, a design procedure has been proposed to proportion the flexure and shear plates of SAFYD devices for a given lateral load demand.

© 2015 Elsevier Ltd. All rights reserved.

1. Introduction

Conventional approach of energy dissipation in a structure is to allow the localized structural damages (i.e., plastic hinges) in the primary lateral load-resisting elements. These damaged elements require either complete replacement or extensive modification in the post-earthquake scenario in order to restore their lateral strength, lateral stiffness, deformability, and energy dissipation/absorption mechanism. A number of innovative techniques have been developed to improve the performance of structures subjected to earthquake excitations by minimizing the damages in the primary load-resisting elements. Traditionally, seismic isolation at the foundation level of a structure is one of the techniques used to increase the structural flexibility, thereby, reflecting a major portion of the earthquake energy [1–4]. The modern techniques of controlling seismic response involve the installation of supplemental energy dissipating/absorbing devices in the structures. The primary aim of adding these supplemental devices in a structure is to dissipate the seismic energy through the hysteretic behavior of specially designed elements and to avoid the localized damages in the primary load-resisting structural elements.

In the past, researchers have proposed a number of passive energy dissipating devices, such as, friction dampers, viscoelastic dampers, metallic yielding dampers, and tuned mass dampers. The working principle, development and concepts, and practical applications of these devices can be found elsewhere [e.g., 5–8]. Metallic yielding dampers are considered to be simple, cost-effective and easy to fabricate. The

main advantages of these devices are symmetric and stable hysteretic behavior, better low-cycle fatigue property, long-term reliability, and relatively insensitive to the environmental actions [9]. Added damping and added stiffness (ADAS) devices are very common metallic dampers in which the hysteretic energy is achieved through the flexural yielding of steel plates [10–12]. Fig. 1(a) shows the typical elevation and sectional views of ADAS devices. A series of steel plates of either triangular or hourglass shapes is placed parallel to each other in these devices allowing the entire cross-section of plates to yield at the same instance [13,14]. For example, the hourglass-shaped plates with rigid connections at both edges deform in double-curvature bending with the magnitude of bending moment varying from a maximum value near the edges to a minimum value at their mid-heights. This leads to plasticization of the entire section of all the plates at the same instance, which enhance the hysteretic energy dissipation potential of ADAS devices.

Another category of metallic dampers, known as shear links, relies on the inelastic shear deformation (i.e., yielding/buckling) of metallic (steel or aluminum) plates under the in-plane loading as shown in Fig. 1(b). Shear yielding of steel (web) plates under the cyclic loading condition results in a stable and excellent hysteretic energy dissipation [15–17]. Aluminum plates are also used as the shear yielding devices due to their low yield strengths and high deformability characteristics resulting in better hysteretic energy dissipation [18–22]. The addition of intermediate stiffeners may delay the inelastic buckling of web (shear) panels and enhance their energy dissipation potential of shear links without pinching even up to 20% shear strain level [19,20]. Aluminum shear links have shown to improve the seismic performance of steel and reinforced concrete (RC) frames in various retrofit projects [23–28]. Recently, a slit-type metallic device fabricated from a short

* Corresponding author.
E-mail address: drsahoo@civil.iitd.ac.in (D.R. Sahoo).

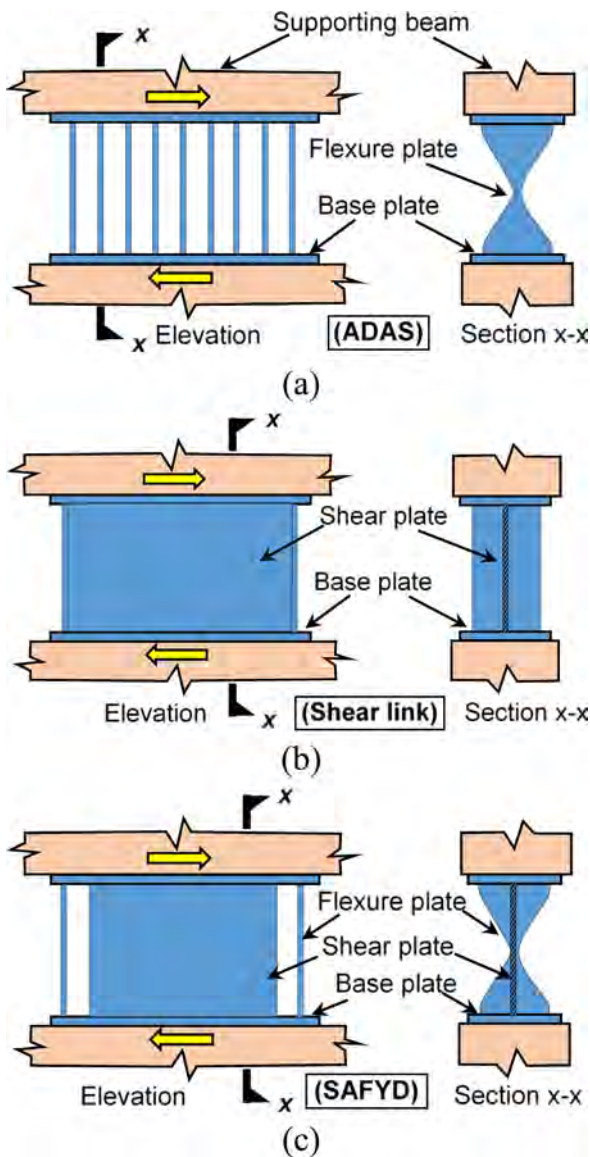


Fig. 1. Geometric details of (a) ADAS device, (b) shear link, and (c) SAFYD.

length of a standard I-steel section with a number of slits cut from the web has been also proposed as passive energy dissipation devices [29]. The steel strips between the two flanges of the I-section are allowed to deform in flexure, thereby dissipating hysteretic energy due to the formation of plastic hinges at their ends. Ghabraie et al. [30] proposed a shape optimization technique for passive metallic devices in order to achieve an even stress distribution and to eliminate the stress concentration in the devices. Karavasilis et al. [31] proposed a hysteretic model for steel energy dissipation devices by modifying the Bouc–Wen model to capture the combined kinematic and isotropic hardening in the hysteresis. Recent studies [32,33] have also shown that the shear yielding devices fabricated from the low yield-strength steel can effectively reduce the damages in long span bridges under seismic loading condition. However, there is still a need of further research to improve the energy dissipation capacity of metallic dampers.

2. Objectives of this study

In the preceding discussions, it is inferred that the energy dissipation potential of a metallic damper primarily relies on its hysteretic response due to the inelastic deformation of metallic plates under

axial or flexural or shear yielding mechanism. The energy dissipation potential of such yielding devices can be enhanced if the metallic plates are so oriented that they can undergo combined inelastic (such as, flexure and shear) deformation under the lateral loading condition. In this study, a combined shear-and-flexure yielding damping (SAFYD) device, as shown in Fig. 1(c), has been proposed as passive energy dissipation system. Both experimental and analytical studies have been conducted to study their performance under slow-cyclic loading. The main objectives of this study are as follows: (i) to investigate the lateral strength, stiffness, ductility and energy dissipation potential of SAFYD devices, (ii) to evaluate the effect of relative size of the shear and flexure plates on the overall performance of these devices, (iii) to study the overall failure mechanism and behavior of connections under cyclic loading, and (iv) to develop an analytical model to predict the cyclic behavior of these devices through validation of experimental results.

3. Concept and design of combined yielding damper

Fig. 2 shows the initial and deformed configurations of SAFYDs under the lateral loading condition. If the top and bottom edges of the flexure (end) plates are rigidly connected to the base plates, these plates will deform in the double-curvature bending similar to the settlement of one end of a fixed-ended beam. The magnitude of bending moment along the depth the flexure plates usually varies from a minimum (zero) value at the mid-section to a maximum value at the edges. If the section modulus of flexure plate of the device is made to vary in proportion to the bending moment along its depth, the entire plate will undergo inelastic deformation at the same instance under the out-of-plane loading. Similarly, the web (shear) plate of the device being subjected to the in-plane loading undergoes the inelastic shear deformation associated with the diagonal tension yielding (T_s) and compression buckling (Fig. 2). The combined flexure and shear inelastic deformations of the flexure and shear plates may result in a better lateral load resistance and energy dissipation of SAFYD devices as compared to the equivalent ADAS or shear link devices. However, due to the significant difference between the flexural and shear stiffness of plates, it may not be possible to achieve the initiation of inelastic deformation (yielding) of the web and end plates simultaneously. Hence, the main challenge is to proportion the flexure and shear plates of SAFYD devices to maximize their overlapping inelastic behavior in the desired range of lateral displacements of structural systems.

The total load (Q) resisted by the SAFYD specimen is the algebraic sum of the loads resisted by the flexural (Q_f) and shear (Q_s) plates assuming these plates to be elastic-perfectly plastic springs connected in series as shown in Fig. 3(a). Since the displacement across these plates along the direction of applied loading is exactly the same, the total stiffness (k) of damper is the algebraic sum of stiffness of the flexure (k_f) and shear (k_s) plates. However, because of the variation in the yielding strength and stiffness between the flexure and shear plates, the computation of design load-resisting capacity of the damper should consider the applicable yielding as well as buckling phenomenon of these plates in the range of design displacements as shown in Fig. 3(b). The yielding

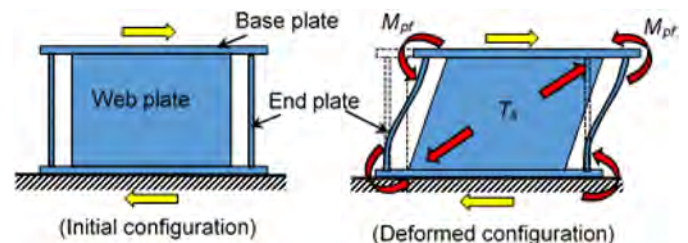


Fig. 2. Energy dissipation mechanism in SAFYD.

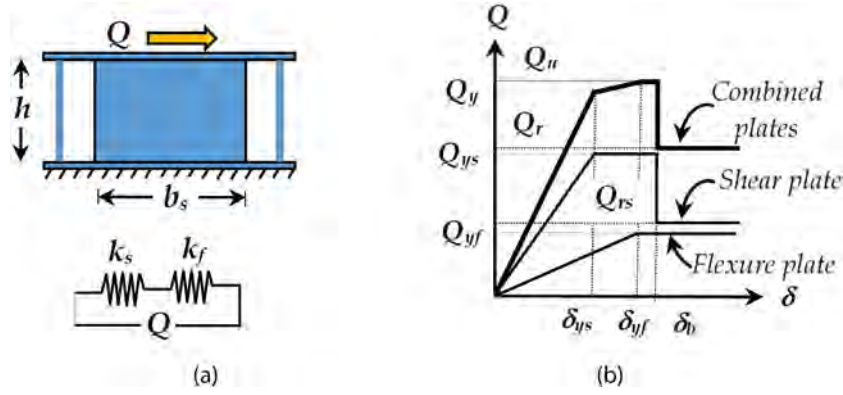


Fig. 3. (a) Equivalent spring model of SAFYD; (b) force–displacement response used in design.

strength (Q_{ys}) and yield displacement (δ_{ys}) of shear plates can be expressed as follows:

$$Q_{ys} = \left(\frac{b_s t_s}{1.2} \right) \left(\frac{f_{ys}}{\sqrt{3}} \right); \quad \delta_{ys} = \left(\frac{h}{G} \right) \left(\frac{f_{ys}}{\sqrt{3}} \right) \quad (1)$$

where, b_s = width of shear plate, t_s = thickness of shear plate, f_{ys} = tensile yield stress of shear plate, h = depth of shear plate, and G = shear modulus of steel. The value of G can be computed as 0.385 times the Young's modulus (E) for a Poisson's ratio value of 0.3. The effective shear area of the plate has been assumed as the total area divided by a factor of 1.2. The stiffness (k_s) of shear plates can be obtained as the ratio of yielding strength to the yield displacement as follows:

$$k_s = \left(\frac{b_s t_s}{1.2} \right) \left(\frac{G}{h} \right). \quad (2)$$

Similarly, the yielding strength (Q_{yf}) of flexural plates can be computed from their yielding moments (M_y) assuming four plastic hinges formed at both ends of two plates as follows:

$$M_y = f_{yf} \left(\frac{b_f t_f^2}{6} \right); \quad Q_{yf} = \left(\frac{4M_y}{h} \right) = f_{yf} \left(\frac{b_f t_f^2}{1.5h} \right) \quad (3)$$

where, b_f = width of flexure plates, t_f = thickness of flexure plates, and f_{yf} = tensile yield stress of flexure plates. Since the width of flexural plates varies along the depth using the average value of plate width. The stiffness (k_f) and yield displacement (δ_{yf}) of flexural plates with fixed ends can be computed as follows:

$$k_f = 2 \left(\frac{12EI_f}{h^3} \right) = \left(\frac{Eb_f t_f^3}{h^3} \right) \quad (4)$$

$$Q_{yf} = k_f \delta_{yf}; \quad \delta_{yf} = 0.67h^2 \left(\frac{f_{yf}}{Et_f} \right). \quad (5)$$

Comparing Eqs. (2) and (5), the value of δ_{ys} will be smaller than the value of δ_{yf} indicating that the yielding of shear plate will occur prior to the flexure plates. Thus, the yielding strength (Q_y) of the damper corresponding to the yield displacement of δ_{ys} can be computed as follows:

$$Q_y = Q_{ys} + k_f \delta_{ys}. \quad (6)$$

The above equation is based on the assumption that the yielding of shear plate will occur prior to its elastic buckling. Therefore, it is necessary to check the elastic as well as inelastic buckling strength of shear plates. Elastic buckling stress (τ_E) of the shear plate can be given by:

$$\tau_E = \frac{k_s \pi^2 E}{12\beta^2(1-\nu^2)} \quad (7)$$

where, k_s = buckling coefficient depending on the edge conditions and aspect ratio ($\alpha = b_s/h$), $\beta = h/t_s$, and ν = Poisson's ratio. The value of k_s for the shear plate with two opposite restrained edges can be computed as follows [34]:

$$k_s = 5.6 + \frac{8.98}{\alpha^2} - 1.99\alpha \quad (\alpha \leq 1) \quad (8a)$$

$$k_s = 8.98 + \frac{5.6}{\alpha^2} - 1.99/\alpha^3 \quad (\alpha \geq 1). \quad (8b)$$

Elastic buckling strength of shear plate is given by as follows,;

$$Q_{se} = \tau_E b_s t_s. \quad (9)$$

The value of Q_{se} is usually greater than Q_{ys} if thin rectangular plates are used as shear plates. The inelastic buckling stress (τ_b) can be computed using tangent modulus theory as follows:

$$\tau_b = \frac{\pi^2 E_t}{\lambda^2}; \quad \text{where, } \lambda = \beta \sqrt{\frac{1.6}{(1+0.7\alpha^2)}}. \quad (10)$$

The value of tangent modulus (E_t) of steel can be assumed as 15% of the value of E . Inelastic buckling strength (Q_{rs}) can be computed as the product of inelastic buckling stress and the gross area of shear plate. The displacement (δ_b) corresponding to the inelastic buckling strength can be estimated using the following expression [35]:

$$\delta_b = 8.7h \left(\frac{k_s}{\beta^2} \right). \quad (11)$$

If the value of δ_b is greater than δ_{yf} , the ultimate strength (Q_u) of the damper can be computed as the algebraic sum of Q_{ys} and Q_{yf} in the pre-buckled stage of the shear plate. At the post-buckled stage, the load resisting capacity (Q_r) of the damper can be estimated as the algebraic sum of Q_{rs} and Q_{yf} . If the value of δ_b is less than δ_{yf} , the value of Q_u and Q_r shall be computed as the algebraic sum of the values of Q_{rs} and Q_{yf} .

Table 1
Details of various components of test specimens.

Specimen	Base plate	Flexure plate	Shear plate
SAFYD-A	270 × 260 × 16	250 × 200 × 6	200 × 200 × 3.2
SAFYD-B	270 × 260 × 16	250 × 200 × 8	200 × 200 × 3.2
SAFYD-C	370 × 260 × 16	250 × 200 × 8	300 × 200 × 3.2

All dimensions are in millimeters.

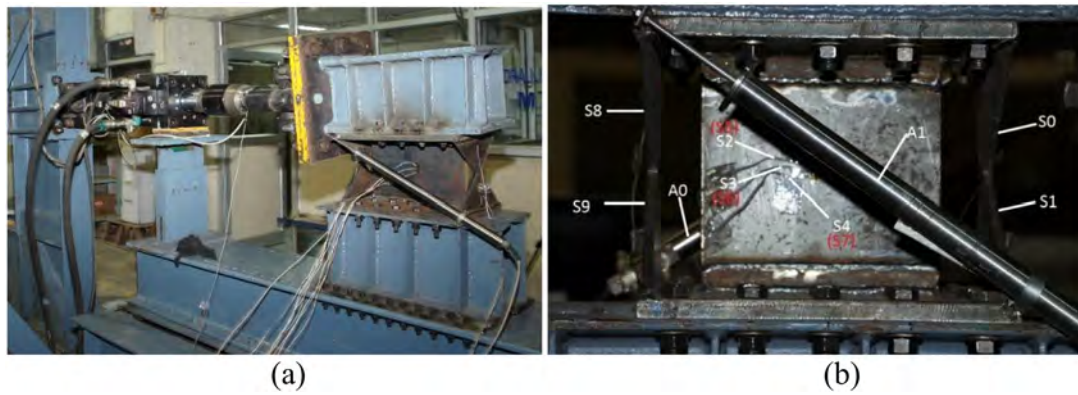


Fig. 4. (a) Test set-up and (b) instrumentations and sensors used in the specimens.

4. Experimental study

An experimental investigation was conducted on a set of SAFYD specimens consisting of two flexure (end) plates of X-shape and a shear (web) plate of rectangular shape. Three test specimens with varying sizes of end and web plates were considered in which both end plates were welded to the bounding base plates at the top and bottom. A parametric study was carried out by varying the sizes of both flexure and shear plates in order to investigate the effect of progressive yielding and relative stiffness of the flexure and shear plates on the overall performance of dampers under the slow-cyclic loading. The details of specimens, fabrication, test set-up, instrumentations and displacement history are discussed in the following sections.

4.1. Test specimens

The overall depth of all specimens was 232 mm including both bases of plates of 16 mm thickness. The size of flexure plates was 250 mm × 200 mm with the thickness of either 6 mm or 8 mm. The web (shear) plates of the specimens consisted of 3.2 mm thick rectangular steel plates of width varying from 200 mm to 300 mm as summarized in Table 1. The increase in thickness of flexure plates or the width of shear plates would result in the higher load resisting capacity of the dampers. The combinations of plate sizes were used to investigate the effect of relative strength (or plastic deformation) on the overall cyclic performance of dampers. Since the thickness of shear plates was small enough making them unsuitable for welding, shear tabs of 20 mm in width and 8 mm in thickness were used at their top and bottom edges. To accommodate the flexural deformation of the end plates in the inelastic range, a gap of 20 mm was intentionally left between the faces of end plates and the edges of shear plates. The width of flexure

plates was gradually reduced to 20 mm at their mid-heights forming X-type configurations.

4.2. Fabrication of specimens

Test specimens were fabricated in-house in the Heavy Structures Laboratory, Indian Institute of Technology Delhi. The web and flexure plates were cut into the desired sizes using a gas flame cutter machine. The flexure plates were cut into X-shapes without any curvature at the re-entrant corners. It should be noted that the gas-cutting process might reduce the ductility property of material near the cutting edges, making the reduced section at the mid-height of the flexure plates more vulnerable to the fracture initiation. First, the flexure plates of desired sizes were connected to the base plates using the multi-pass fillet welds. The maximum size of fillet welds used between the flexure and base plates was limited to 1.5 mm less than the smaller thickness of plates. Next, the shear tabs were placed at the center of base plates and the fillet welds were used on both sides at their interfaces. Finally, the shear plates were connected to these shear tabs using the fillet welds running along the entire length on both sides to complete the assembly of specimen. In addition, sufficient number of bolt-holes was made on the base plates in order to facilitate the connection of specimens with the test set-up.

4.3. Test set-up

Fig. 4(a) shows the test set-up used in the slow-cyclic testing of specimens. The bottom base plate of specimen was attached to the test bed fabricated using rolled steel I-girders firmly attached to the laboratory strong floor. For this purpose, high-strength bolts 12 mm diameter were used in four rows, which simulated the fixed boundary condition

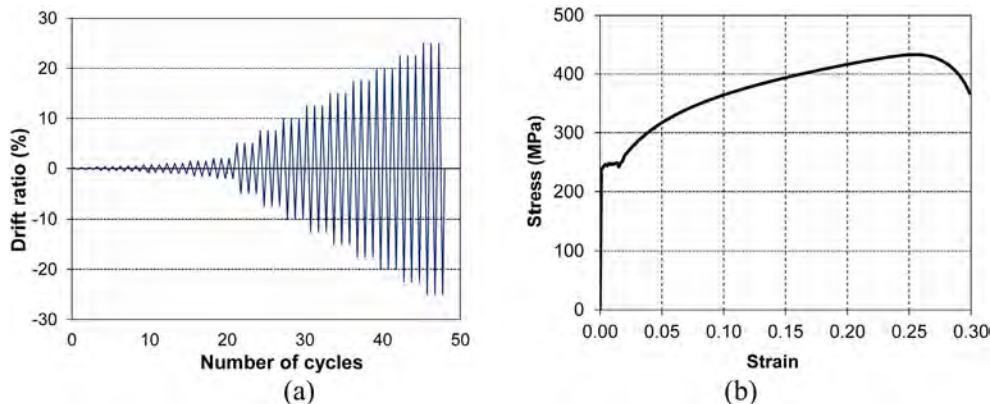


Fig. 5. (a) Displacement history used in this study; (b) tensile stress-strain response of steel.

Table 2
Tensile stress–strain properties of steel coupons.

Plate type	Sample no.	Yield stress (MPa)	Ultimate stress (MPa)	Ultimate strain (%)
Shear plate	1	233.3	340.7	21.4
	2	239.2	342.9	20.8
	3	237.8	342.5	21.2
	Average	236.8	342.0	21.1
Flexure plate	4	299.1	445.6	19.7
	5	296.3	442.2	19.4
	6	297.2	443.8	18.8
	Average	297.5	443.9	19.8

at their bases of specimens. A displacement-controlled cyclic loading was applied using a servo-controlled hydraulic actuator of 250 kN force capacity and 125 mm stroke length. One end of the actuator was attached to a reaction frame, whereas the other end of the servo-controlled actuator was attached to the top base plate of specimen by means of a connector beam. The connector beam was not restrained against the out-of-plane movement assuming that the in-plane stiffness of two end plates would provide sufficient rigidity against the out-of-plane displacement. The attachment of actuator with the connector beam was made in such a way that the lateral load was applied uniformly over the top base plate of the specimen causing the flexural deformation of end plates and the shear deformation of web plate.

4.4. Instrumentations and sensors

The load cell and displacement sensors of the servo-controlled actuator were used to measure the magnitude of the lateral load resistance capacity of the specimen and the corresponding applied displacement level, respectively. The state of strain in the flexure and shear plates of the specimens was monitored during the testing. Several uniaxial strain gauges and strain-rosettes were used at the critical locations of the specimens. Fig. 4(b) shows the instrumentations and sensors used in the specimens during the slow-cyclic testing. Two uniaxial electrical-resistance (120-Ohm) strain gauges were used to monitor the magnitude of flexural strain at the top and bottom ends of each flexure plate. Thus, a total of four strain gauges (S0, S1, S8, S9) were placed on the end plates. Two 45°-strain rosettes consisting of six strain gauges (S2, S3, S4, S5, S6, S7) were placed at the center of the web plate to monitor the state of shear strain at the different stages of loading. The diagonal (shear) displacements of panels were measured using two displacement sensors (A0,A1) on both sides of the specimens as shown in Fig. 4(b). Both these sensors were placed in diagonally opposite directions to measure the panel deformation. All these sensors were connected to an automatic data-acquisition system to monitor the real-time response of the specimens and to record the data measured during the testing.



Fig. 6. Steel coupons used in tensile testing (a) original specimens and (b) tested specimens.

4.5. Displacement history

Test specimens were subjected to a gradually-increased reversed-cyclic displacements as per FEMA-461 [36] specimens at the top plate level. As shown in Fig. 5(a), the magnitude of cyclic displacement excursions was varied in the range of 0.2–24% drift ratio. Drift ratio can be defined as the ratio of the displacement of specimen at the top base level along the loading direction to the overall height of test specimens. Each displacement cycle at any drift ratio level was repeated for three cycles in order to monitor the repetitive response of the specimens. Each specimen was subjected to the cyclic displacement excursions of increasing magnitude till a significant reduction in the lateral strength/stiffness was noticed or the specimen became unstable under the applied loading conditions. It is worth mentioning that drift ratio values also represent a measure of shear strain in the web plate of specimens.

4.6. Material properties

Since the base plates were not expected to undergo the inelastic deformations, the lateral strength and energy dissipation potential of SAFYD specimens primarily depend on the configuration of flexure and shear plates. Tensile testing of steel coupons was conducted to determine the stress–strain behavior of steel used as flexure and steel plates as per IS:1608 [37] specifications. Table 2 summarizes the values of yield stress, ultimate stress, and ultimate strain of steel coupons. Three coupons from each plate (i.e., shear and flexure) were tested under the monotonic increased loading at a rate of 3 mm/min until the failure. Fig. 5(b) shows the typical tensile stress–strain response of steel coupons. The modulus of elasticity of steel was found to be about 210 GPa. The average values of material tensile yield stress of shear and flexure plates were computed as 236.8 MPa and 297.5 MPa, respectively. The corresponding values of ultimate tensile stresses were found to be 342.0 MPa and 443.9 MPa. However, both the flexure and shear plates exhibited a maximum tensile strain of 20%. The relatively smaller values of yield and ultimate stress noted for the thinner plates as compared to the thick plates indicate the variations in chemical composition of steel used for these plates. Fig. 6 shows the steel coupons before and after the tensile testing.

5. Test results

The main parameters evaluated are hysteretic response, ultimate strengths, failure/yield mechanism, energy dissipation potential, and behavior of connections as discussed below.

5.1. Hysteretic response

Fig. 7 shows the lateral strength vs. drift response of all three specimens tested in this study. All specimens exhibited nearly linear elastic behavior up to 2.0% drift ratio beyond which the inelastic deformation was noticed in the hysteretic response. Since the shear stiffness of web plates was significantly higher than the flexural stiffness of end plates, the hysteretic behavior of the specimens during the initial cycles was largely controlled by the inelastic deformation of shear plates. Both SAFYD-A and SAFYD-B specimens exhibited the same value of yield strength indicating that the increase in the thickness of flexure plates had no significant influence on the yielding strength of specimens. As expected, the specimen SAFYD-C exhibited a relatively higher yield strength due to the larger size of web plate. All the specimens reached their ultimate strengths at drift ratio of 5.0% beyond which a gradual reduction in their load resisting capacity was noticed due to the initiation of inelastic buckling of the web plate. Specimen SAFYD-A exhibited a sudden reduction in the load resisting capacity at a drift ratio of 7.5% where the welding failure between the web plate and the base plate was noticed. The lateral load resistance of specimen SAFYD-A was

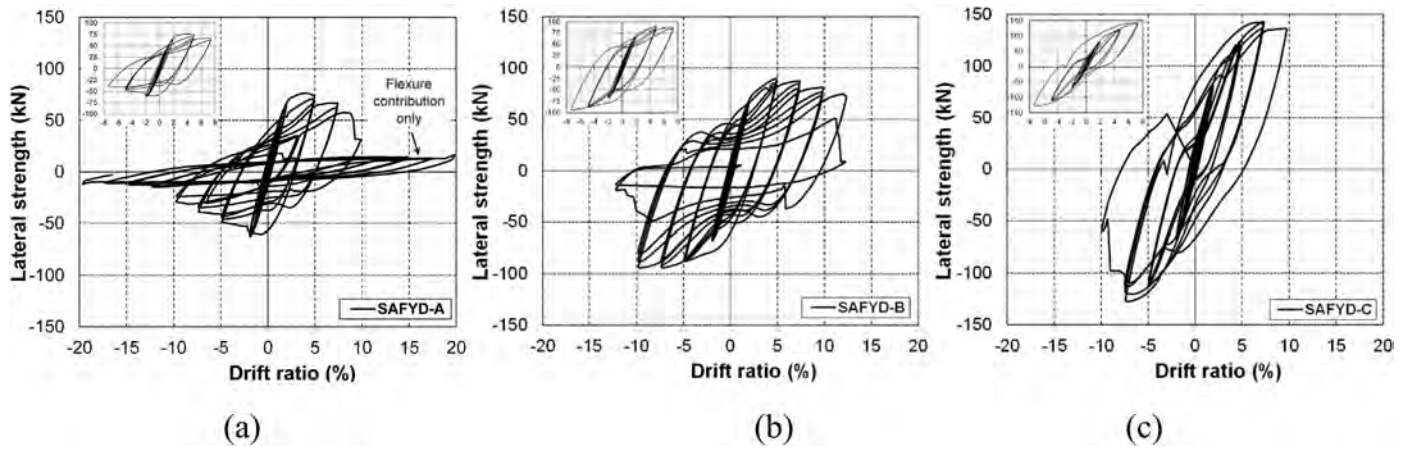


Fig. 7. Hysteretic response of test specimens: (a) SAFD-A, (b) SAFYD-B, and (c) SAFYD-C.

then provided by the flexure plates without any further strength degradation till a drift ratio of 20%. The maximum lateral load resisted by the flexure plates was about 35% of the ultimate resistance indicating a significant contribution from the web plate. The specimen SAFYD-B showed excellent hysteretic response without significant degradation in the strength and stiffness up to a drift ratio of 12.5% where the fracture of end plates was noticed at their mid-height. Similar fracture of end plates was also noticed for the SAFYD-C specimen beyond a drift ratio of 10%.

5.2. Lateral strength

Fig. 8(a) shows a comparison of the backbone curves of load–displacement response of test specimens. The lateral load values plotted in the figure represent the average value of lateral loads resisted by the specimens during three repetitive displacement cycles at a particular drift ratio level. Specimens SAFYD-A and B showed the same linear elastic stiffness and load resisting capacity up to 2.0% drift ratio. The corresponding yield strengths of these specimens were noted as 64 kN and 68 kN, respectively. It should be noted that no significant difference in magnitude of yield strengths was noted although a higher thickness of flexure plate was used in the SAFYD-B specimen as compared to the SAFYD-A. However, the specimen SAFYD-C exhibited the higher initial elastic stiffness and the load resisting capacity at all drift levels. This is primarily because of the larger size of web plate used in the specimen. The maximum load resisted by the specimen SAFYD-C was noted as 75 kN at drift ratio of 2%, beyond which the inelastic (shear) deformation was noted in the web plates of all specimens except the specimen

SAFYD-A. The strength-degradation effect as noted Fig. 8(a) for the specimen SAFYD-A was primarily due to the failure of connection between the shear plate and the base plates. The maximum lateral load resisted by the flexure plates of specimen SAFYD-A was found to be about 15 kN which is about 23% of the peak load beyond 10% drift ratio. Specimen SAFYD-B exhibited the strain-hardening behavior in the hysteretic response till a drift ratio of 7.5% showing a peak load of 88 kN. Beyond this drift level, a gradual reduction in the load resistance is noticed for the specimen till a drift ratio of 12.5% where the failure of flexure plates was noted. A significant strain-hardening behavior was observed in the load–displacement curves of the specimen SAFYD-C till 7.5% drift ratio, where the maximum load resisted by the specimen was found to be 132 kN followed by a reduction in the load resistance. As compared to the specimen SAFYD-B, an increase of 50% in the load resistance was noted for the specimen SAFYD-C where the size of web plate was larger by the same proportion. Hence, in order to achieve a higher lateral load resistance, a larger width of web plate should be used instead of the thicker flexure plates. However, a parametric study needs to be carried out to determine the relative size of web and flexure plates in order to get a desired level of deformability without any instability.

5.3. Energy dissipation and damping

The energy dissipation potential of test specimens was computed as the area enclosed within the load–displacement curves at a particular drift level. Since each drift cycle was repeated three times, the total energy dissipated by a specimen at any drift cycle would represent the

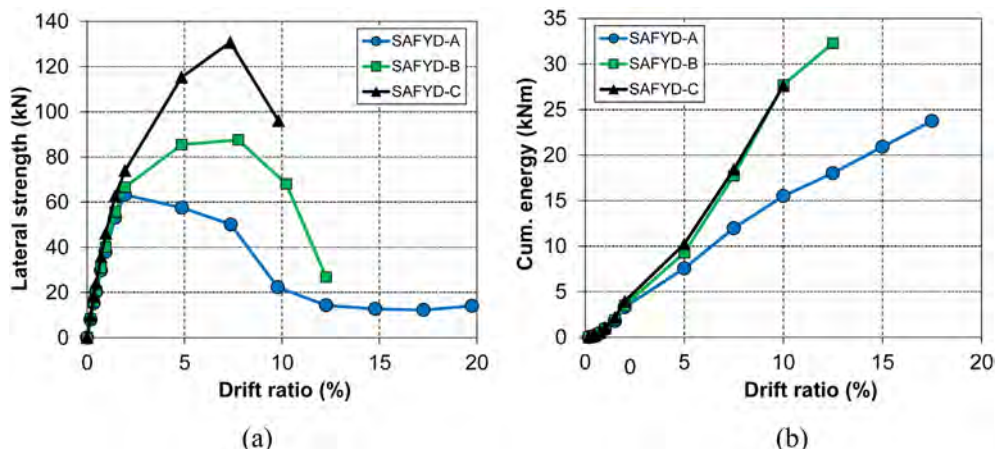


Fig. 8. (a) Backbone curves and (b) cumulative energy dissipation response of specimens.

Table 3
Computation of equivalent damping of test specimens.

Drift ratio (%)	SAFYD-A				SAFYD-B				SAFYD-C			
	Δ_{av} (mm)	K_{eff} (kN/mm)	E_{cycle} (kN/mm)	ζ (%)	Δ_{av} (mm)	K_{eff} (kN/mm)	E_{cycle} (kN/mm)	ζ (%)	Δ_{av} (mm)	K_{eff} (kN/mm)	E_{cycle} (kN/mm)	ζ (%)
0.19	0.35	22.67	5.58	31.84	0.36	23.17	5.88	31.76	0.36	26.52	6.70	31.67
0.38	0.68	22.26	20.70	31.71	0.70	22.68	22.52	31.81	0.70	26.12	25.72	31.61
0.50	0.92	21.83	37.28	31.87	0.93	22.37	39.15	31.95	0.93	25.91	44.82	31.61
0.75	1.43	20.83	84.84	31.80	1.43	21.67	88.40	31.78	1.44	24.99	102.66	31.73
1.00	1.89	20.01	142.84	31.66	1.91	20.97	153.36	31.89	1.91	24.15	177.57	31.95
1.50	2.87	18.45	303.76	31.76	2.88	19.40	324.56	32.20	2.87	21.78	366.40	32.41
2.00	3.89	16.28	508.11	32.88	3.88	17.17	537.71	33.08	3.89	19.00	589.00	32.55
5.00	9.73	5.91	1420.44	40.40	9.70	8.82	1922.69	36.90	9.69	9.95	2098.89	35.73
7.50	14.75	3.40	1468.06	31.60	15.51	5.64	2822.68	33.10	14.68	6.39	2735.39	31.60
10.00	19.56	1.14	1180.59	43.07	20.44	3.33	3322.83	37.99	19.64	4.12	3061.15	30.64
12.50	24.53	0.58	834.50	37.80	24.52	1.09	1532.44	37.07	-	-	-	-
15.00	29.56	0.43	968.81	40.98	-	-	-	-	-	-	-	-
17.50	34.53	0.36	942.08	35.42	-	-	-	-	-	-	-	-

cumulative energy dissipation value. Fig. 8(b) shows the cumulative energy dissipated by the specimens at different drift ratio levels. As expected, the specimen SAFYD-A exhibited smaller energy dissipation where the cumulative energy vs. drift response was nearly linear. The maximum values of energy dissipated by the specimen SAFYD-A were noted as 23 kN/mm at a drift ratio of 17.5%. Both specimens SAFYD-B and C exhibited almost similar energy dissipation response where the energy vs. drift response was approximately exponential till a drift ratio of 10%. Specimen SAFYD-C showed a marginally higher value of energy dissipation at each drift level as compared to the specimen SAFYD-B. However, both specimens dissipated the same magnitude (~28 kN/mm) of energy at a drift ratio of 10%, which was nearly 85% higher than that dissipated by the specimen SAFYD-A at the same drift level indicating the higher energy dissipation due to the use of wider web plate.

The energy dissipated per cycle at each drift level was used to compute the hysteretic damping of the specimens. The magnitude of equivalent viscous damping (ζ) was computed as follows [38]:

$$\zeta = \frac{E_{cycle}}{2\pi K_{eff} \Delta_{av}^2} \tag{12}$$

where, E_{cycle} = energy dissipated per cycle at any drift level, K_{eff} = effective stiffness = $(F^+ - F^-)/(D^+ - D^-)$, F = peak load resisted by the specimen, D = maximum displacement in the cycle, and Δ_{av} = average displacement in the cycle = $(D^+ - D^-)/2$. Superscripts (+/-) represent the positive/negative directions of loading. Table 3 summarizes the equivalent viscous damping values of the specimens at different drift cycles. The magnitude of damping varied from 30.7 to 43.1% for the specimen SAFYD-A. The maximum damping value of 43.1% was noted at 10% drift ratio. During the initial (elastic) drift ratio cycles, all

specimens showed an equivalent damping of about 31.0%. The magnitude of damping was gradually increased to a value of 38% at drift ratio of 10% for the specimen SAFYD-B. Similarly, the specimen SAFYD-C exhibited a maximum equivalent damping of 35.73% at a drift ratio of 5%.

5.4. State of strain

The state of strain in the flexure and shear plates of the specimens was monitored using the uniaxial strain gauges. The flexure plates were fitted with uniaxial strain gauges at both ends, whereas the shear plates were fitted with 45°-strain rosettes at the mid-sections. Fig. 9(a) shows the typical load–strain variation in the end plates of test specimens up to 2% drift ratio. The load–strain response was nearly linear till 0.375% drift ratio beyond which the widening of loops was noted. At 1.5% drift ratio level, the widening of load–strain response was noticed in the reversed direction indicating the initiation of the double-curvature bending of the end plate. Due to the excessive deformation of end plates, the detachment of strain gauges was noted at the higher drift levels beyond the drift ratio of 7.5%. Fig. 9(b) shows the average value of the maximum strain recorded during the three cycles at any drift level in both directions of loading. Considering the average yielding strain value of 0.15%, all specimens yielded just beyond the 2% drift ratio level. The maximum value of strain reached by specimen SAFYD-A was 0.5% at a drift ratio of 7.5%, whereas the maximum strain reached by the specimen SAFYD-C was 0.25% at the same drift ratio level. This shows that increasing the size of shear plate reduces the flexural strain demand on the end plate of test specimens. Initially, minor difference in the average strain values was noted between the top and bottom regions of the end plates, which gradually diminished at the

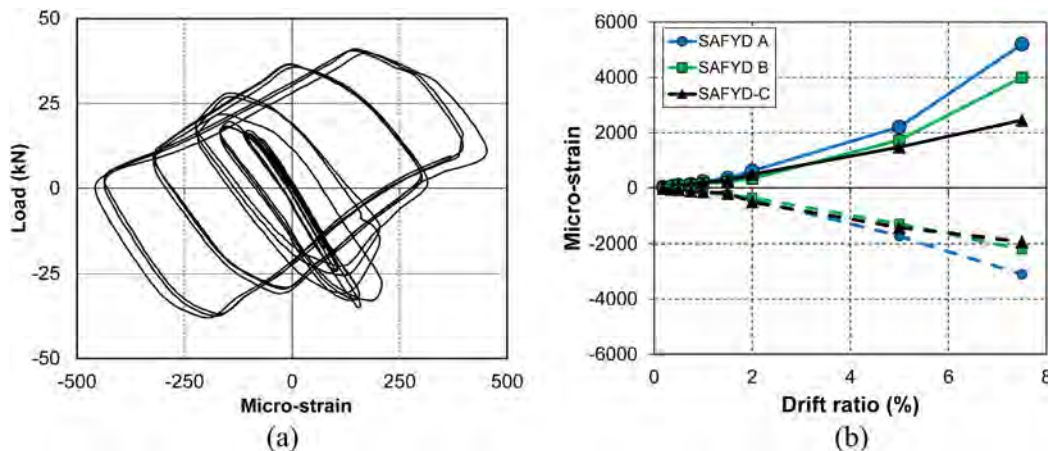


Fig. 9. (a) Load–strain response of end plates, (b) variation of strain with the drift cycles.

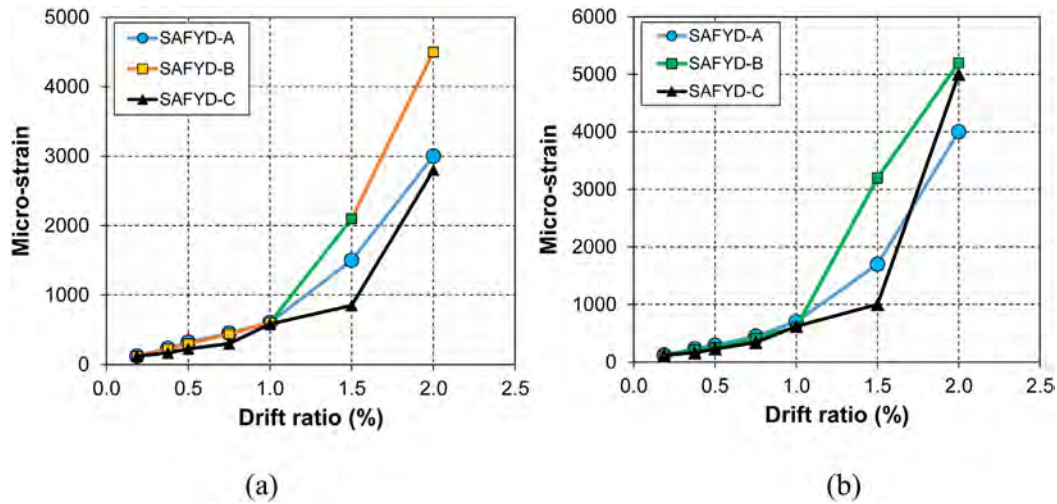


Fig. 10. State of strain in the web plates (a) principal strain and (b) shear strain.

higher drift cycles. As expected, the magnitude of flexural strain was increased with the increased drift values. Thus, the yielding of the entire cross-sections of the end plates was noticed indicating more utilization of material in the energy dissipation.

The state of strain in the web plates of test specimens was monitored through the strain values along three axes using 45°-strain rosettes. The principal strain and shear strain in the web plates were computed using the strain transformation theory. Fig. 10 shows the average values of principal strain and shear strain in the web plates of all specimens. As compared to the end plates, the inelastic deformation of shear plates was noted at very low drift levels. Hence, the principal strain and shear strain values were computed only up to 2% drift level. As shown in Fig. 10(a), the web plates of all specimens reached the tensile yield limit of 0.15% at about 1.5% drift ratio level. SAFYD-B specimen reached a maximum principal strain of 0.45% at 2% drift ratio level. Using von-Mises failure criteria, the value of yield strain in shear can be computed as 0.22%. As shown in Fig. 10(b), the web plates of all specimens reached the shear yielding limits at the same drift level as the principal strain. Specimen SAFYD-B exhibited a maximum shear strain of 0.5% at 2% drift ratio level. The values of principal strain and shear strain for the specimen SAFYD-C were relatively smaller as compared to the other specimens.

5.5. Yield mechanism and connection behavior

As expected, shear yielding of web plates was noticed prior to the flexure plates in all test specimens. Since the web plates were unrestrained on their vertical edges, the out-of-plane displacement of these plates was noticed during the initial drift cycles. At 1.5% drift ratio cycles,

the outward bulging of shear plates was noticed near the mid-regions, like a saucer shape, due to the formation of compression strut under the cyclic loading. At 2.0% drift ratio, shear buckling of web plates was initiated in all specimens. At the same instance, the flexural yielding of end plates was also noticed. Fig. 11(a) shows the failure mechanism of specimen SAFYD-A. The failure of welding connection between the web plate and the base plate was observed in the specimen SAFYD-A at drift ratio of 7.5%, beyond which the lateral resistance was offered only by the end plates. Specimen carried the lateral load till 20% drift ratio level at which the fracture of end plates was noticed. Fig. 11(b) shows the failure mechanism of specimen SAFYD-B. The tearing of shear plates was noticed at the weld locations near the edges. At 12.5% drift ratio level, fracture of flexure plates of SAFYD-B specimen was observed at the mid-height initiated due to the weld failure at the interface between the end plate and base plate as shown in figure. Since the localized heating due to gas-flame cutting of plates increase their yield/ultimate strengths and reduce their ductility, this might have induced the brittle fracture of plates under cyclic loading. However, in the case of the full-scale SAFYD specimens, this effect would be small as compared to the small-scale specimens used in this study. Further, the cutting edges at the mid-heights of end plates had the reentrant corners that might also have initiated the fracture in these plates. Fig. 11(c) shows the failure mechanism of the specimen SAFYD-C where instability occurred owing to the twisting of specimen. This is primarily due to the eccentricity between the reentrant corners at the mid-heights of end plates due to unsymmetrical cutting of plates. However, this situation would not arise in practical application, since both base plates would be restrained by the connecting frame members. Nevertheless, the following detailing of end plates may enhance the

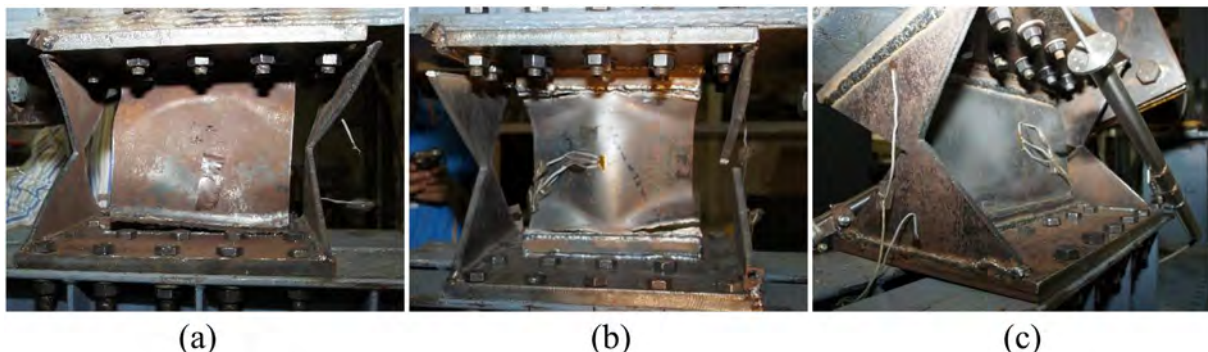


Fig. 11. Modes of failure of specimens: (a) SAFYD-A, (b) SAFYD-B, and (c) SAFYD-C.

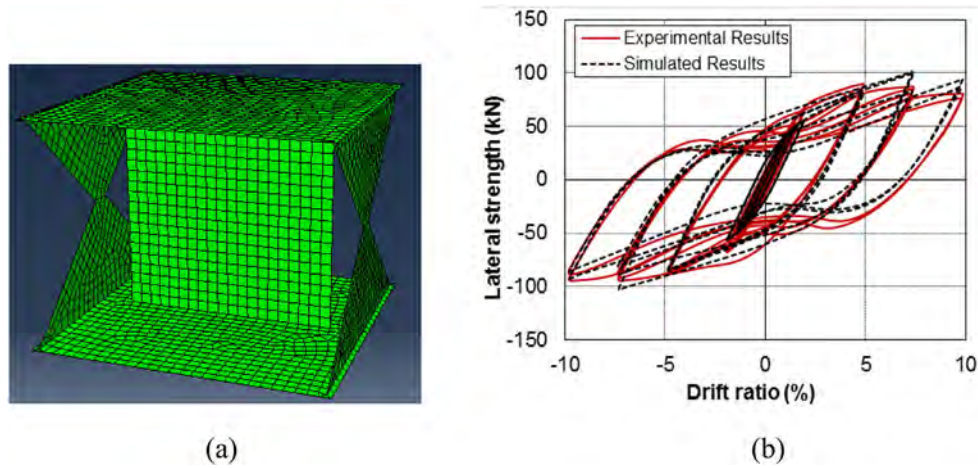


Fig. 12. (a) Finite element model of specimen SAFYD-B, (b) comparison of hysteretic response.

cyclic performance of SAFYD specimens: (a) each plate should be prepared from machine cutting without any reentrant corners (e.g., hourglass shape); and (b) end plates should be perfectly symmetric in order to avoid the eccentric stress distribution under lateral loading.

6. Discussion

A finite element study was conducted to predict the lateral strength and cyclic response of SAFYD devices. In addition, the experimentally obtained results were also compared with the design values as discussed in the following sections:

6.1. Analytical prediction of cyclic response

An analytical study was also conducted to predict the cyclic performance of SAFYD-B specimen using finite element analysis software, ABAQUS v.6.10 [39]. Quadrilateral four-node double-curved shell (S4R) elements were used to model all the components of the specimen. The S4R element has three translational and three rotational DOFs at each node and uses a reduced-integration scheme with just one integration point at the center of the element as opposed to three points for the higher order elements. The true stress–strain values derived from the coupon test results were assigned as the material properties to these elements. The bottom base plate was assumed to be perfectly fixed, whereas the gradually-increased cyclic displacements was applied to the top base plate. Finite element mesh was generated by seeding the

edges depending upon the fineness of the mesh required. Based on a mesh convergence study, shell (S4R) elements of 10 mm size were used to mesh the entire model using free meshing technique. Specifically, the medial axis theorem was used for the structured meshing in which the region to be meshed was divided into a number of small regions and the structured meshing was carried out in the small regions with more elements as shown in Fig. 12(a). The localized heating effect as well as welding connections was not explicitly modeled in this study. Instead, the rigid connections between elements in the interface regions were assumed in the finite element model. Further, the presence of shear tabs near the edges of shear plates was considered by increasing the thickness of elements in these regions.

Fig. 12(b) shows a comparison of simulated hysteretic response with the test result of specimen SAFYD-B. The analysis result matched very well with the experimental data. The strength and stiffness degradation behavior of the specimen in the repetitive cycles of the higher drift levels was also noticed in the analysis. A little larger load carrying capacity was noticed during first two cycles of 7.5% drift level in the analysis model, the maximum difference being in the order of 10%. The lateral load resisted by the analytical model was found to be nearly the same as the experimental data at each drift level in the pull (compression) side of loading. Thus, the adopted finite element model successfully captured the load–deformation behavior of the damper. Fig. 13(a) shows the comparison of the backbone curves of load–deformation behavior of model with experimental results. The average value of the predicted lateral strength at each drift level was found to be nearly the same as that obtained from the experiment with a maximum variation of 8%.

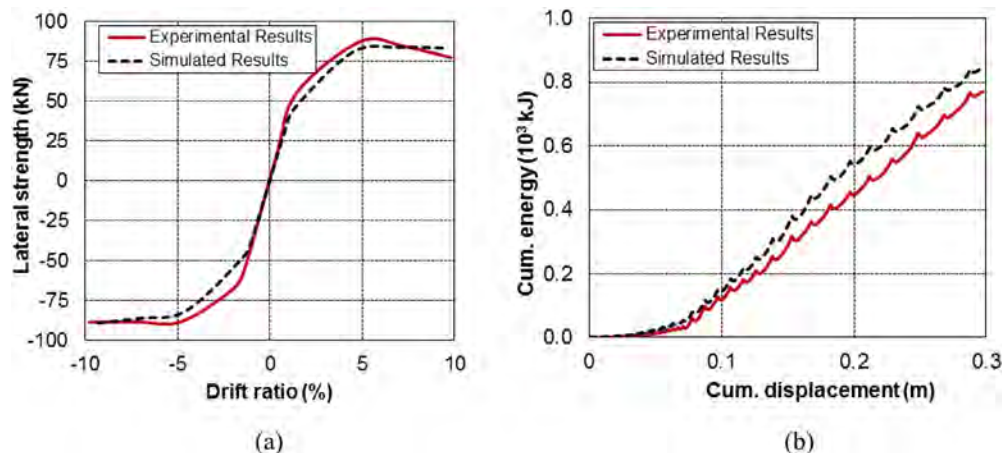


Fig. 13. Comparison of (a) backbone curves and (b) cumulative energy dissipation of SAFYD-B.

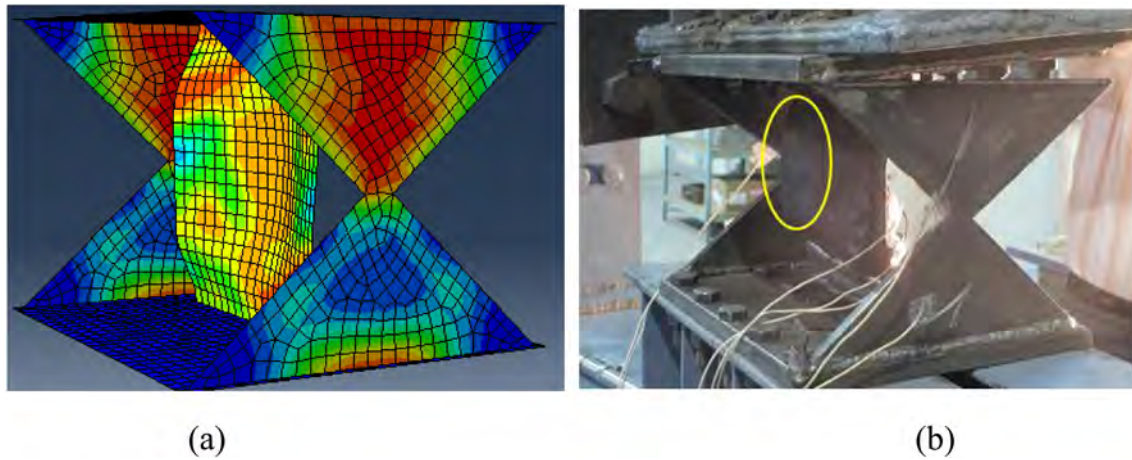


Fig. 14. Comparison of deformed shapes of specimen SAFYD-B (a) simulation and (b) experiment.

Thus, a reasonably good match was also noticed between the experimentally obtained and predicted backbone curve of load–deformation behavior of the specimen. Fig. 13(b) shows the comparison of cumulative energy dissipated by the test specimen and the model. The finite element model predicted a little larger amount of energy ($\sim 8.5 \times 10^3$ kJ) as compared to the experimental value of 6.8×10^3 kJ. The difference in energy dissipation may be attributed to the eccentricity due to the stiffening plates (shear tabs) and residual stresses developed during cutting and welding of flexure and shear plates of the specimen, which were not considered in the finite element model. Fig. 14 shows a comparison of the deformed configuration obtained from analysis and experiment. The out-of-plane deformation of web plate noticed both in the finite element analysis as well as in the experiment. Hence, the energy dissipation and the deformed configuration of the devices can be reasonably predicted by finite element analysis. However, a detailed finite element modeling is required to predict the fracture behavior of test specimens.

6.2. Comparison of experimental results with design values

The design yield and ultimate strengths of test specimens were computed using the methodology discussed in Section 3. Table 4 summarizes the design strengths and corresponding displacements of test specimens. The average value of tensile stress of shear plates and flexure plates was used in the computation of the design strengths. The yield strengths of shear plates of all specimens were higher than the elastic buckling strengths. Both SAFYD-A and SAFYD-B specimens had exactly the same design yield and inelastic buckling strengths of shear plates because of their exactly the same configurations. Similarly, SAFYD-B and SAFYD-C specimens had equal flexural strengths. The design ultimate strength of SAFYD-C specimen was higher than the corresponding values for other two specimens. As compared to the SAFYD-B specimen, an increase of nearly 50% in the ultimate strength noted for the specimen SAFYD-C was primarily due to the about 50% increase in the area of shear plate. Further, since the design inelastic buckling strength of the shear plate was higher than the corresponding yield strength, the post-buckled strength of the SAFYD-C specimen was higher than the ultimate strength by about 10% indicating no degradation in the load-resisting capacity. It is worth mentioning that the strain-hardening behavior of the material was not considered in the design for simplicity. A comparison

of experimental results with the design values is summarized in Table 5. The yield strengths of test specimens obtained from the experiment were nearly the same as the design values except for the specimen SAFYD-C where nearly a maximum difference of 30% in the actual and design values was noted. The out-of-plane behavior of the specimen due to the presence of eccentricity in the flexural plates might have induced the early yielding shear plates. Further, the presence of residual stress in the plates may also cause a reduction in the yield strengths. The actual values of ultimate strengths were nearly the same as the design values of specimens. The specimen SAFYD-C exhibited a little higher value of ultimate strengths as compared to the design value. However, due to the premature failure of web and end plates, the actual post-buckled strengths of the test specimens were much smaller than the design values. It should be noted that the ratio of stiffness of shear plate to the stiffness of flexure plate of SAFYD-C specimen was nearly 100 (Table 4) where the higher ultimate strength with no strength-reduction was noticed. In contrast, specimen SAFYD-A having a stiffness ratio of nearly 150 exhibited premature failure of shear plate without any significant strain-hardening behavior. Based on this limited study, the size of flexural and shear plates used in the specimen SAFYD-C was found to exhibit better energy dissipation. Nevertheless, further refinement in the design procedure is required which must be calibrated through experimental investigation of additional number of test specimens.

7. Conclusions

The following conclusions can be drawn from the present study:

- The combination of shear and flexural yielding of plates in metallic dampers significantly increases the lateral load carrying capacity and the energy dissipation potential as compared to the ADAS and shear link devices. A considerable saving in materials and cost can be achieved in the case of SAFYD devices for the same level of lateral strength and energy dissipation.
- The addition of thin web (shear) plate in ADAS devices improves the lateral stiffness and lateral strength of the devices. The ratio of lateral strength and stiffness of the flexure (end) plates to the shear (web plate) in post-yield regions is about 20–30%. A higher value of lateral strength, energy dissipation, and damping can be achieved by

Table 4
Design strengths of test specimens.

Specimen	Q_{ys} (kN)	δ_{ys} (mm)	Q_{yf} (kN)	δ_{yf} (mm)	Q_b (kN)	δ_b (mm)	Q_y (kN)	Q_u (kN)	Q_r (kN)	Ratio Q_r/Q_u	Ratio k_s/k_f
SAFYD-A	72.9	0.34	8.9	6.3	54.1	5.61	73.4	80.9	63.0	0.8	152
SAFYD-B	72.9	0.34	15.9	4.7	54.1	5.61	74.1	88.8	70.0	0.8	64
SAFYD-C	109.4	0.34	15.9	4.7	123.0	4.85	110.5	125.2	138.8	1.1	96

Table 5

Comparison of experimental results with design values.

Specimen	$Q_{y,exp}$ (kN)	$Q_{u,exp}$ (kN)	$Q_{r,exp}$ (kN)	Ratio $Q_y/Q_{y,exp}$	Ratio $Q_u/Q_{u,exp}$	Ratio $Q_r/Q_{r,exp}$
SAFYD-A	64.0	66.0	16.0	0.87	0.82	0.25
SAFYD-B	68.0	88.0	28.0	0.92	0.99	0.40
SAFYD-C	75.0	132.0	95.0	0.68	1.05	0.68

increasing in the width of shear plate, rather than increasing the size of flexure plates.

- X-shaped flexure plates with reentrant corners at the mid-height of SAFYD devices can help in dissipating hysteretic energy up to 12.5% drift level without fracture. However, the fracture resistance can be enhanced by avoiding the reentrant corners at the mid-section.
- The prediction of cyclic behavior of SAFYD devices can be carried out to a reasonable accuracy by finite element analysis using commercially available software ABAQUS. Lateral strength, energy dissipation capacity and deformed configurations of SAFYD devices matched very well with those obtained from experimental investigation. However, further study is required to establish the relationship between the relative size of shear and flexure plates for the efficient utilization of materials in achieving better energy dissipation potential.

Acknowledgments

The authors would like to thank the Department of Science and Technology, Government of India (Grant no. SR/FTP/ETA-0041/2011) for the financial assistance in conducting this research. The help and support received from Structural Engineering Laboratory Staff of IIT Delhi is also greatly acknowledged.

References

- [1] I.G. Buckle, R.L. Mayes, Seismic isolation history, application, and performance-world view, *Earthquake Spectra* 6 (2) (1990) 161–201.
- [2] J.M. Kelly, *Base Isolation: Origins and Development*, Earthquake Engineering Research Center, University of California, Berkeley, California, 1991.
- [3] A. Mokha, M.C. Constantinou, A.M. Reinhorn, V. Zayas, Experimental study of friction pendulum isolation system, *ASCE J. Struct. Eng.* 117 (4) (1991) 1201–1217.
- [4] M.C. Constantinou, A. Kartoum, A.M. Reinhorn, P. Bradford, Experimental and theoretical study of a sliding isolation system for bridges, Report No. NCEER 91-0027, National Center for Earthquake Engineering Research, Buffalo, New York, 1991.
- [5] I. Olariu, Passive control and base isolation: state-of-the-art lecture, in: Duma (Ed.), *Proc. Tenth European Conf. Earthq. Eng. Balkema*, Rotterdam 1994, pp. 703–713.
- [6] G.W. Housner, L.A. Bergman, T.K. Caughey, A.G. Chassiakos, R.O. Claus, S.F. Masri, R.E. Skelton, T.T. Soong, B.F. Spencer, J.T.P. Yao, *Structural control: past, present, and future*, *ASCE J. Eng. Mech.* 123 (9) (1991) 897–971.
- [7] M.C. Constantinou, T.T. Soong, G.F. Dargush, *Passive Energy Dissipation Systems for Structural Design and Retrofit*, Monograph, Multidisciplinary Center for Earthq. Eng. Res, University at Buffalo, New York, 1998 (299 pp.).
- [8] F. Naeim, J.M. Kelly, *Design of Seismic Isolated Structures*, John Wiley, New York, 1999 (289 pp.).
- [9] J.M. Kelly, R.L. Skinner, A.J. Heine, Mechanisms of energy absorption in special devices for use in earthquake-resistant structures, *Bull. N. Z. Nat. Soc. Earthq. Eng.* 5 (3) (1972) 63–88.
- [10] A.S. Whittaker, V.V. Bertero, C.L. Thompson, L.J. Alonso, Seismic testing of steel plate energy dissipation devices, *Earthquake Spectra* 7 (4) (1991) 563–604.
- [11] D.M. Bergman, S.C. Goel, Evaluation of cyclic testing of steel-plate devices for added damping and stiffness, Rep. No. UMCE 87-10, Univ. of Michigan, Ann Arbor, 1987.
- [12] K.C. Tsai, H.W. Chen, C.P. Hong, Y.E. Su, Design of steel triangular plate energy absorbers for seismic-resistant construction, *Earthquake Spectra* 9 (3) (1993) 505–528.
- [13] C. Xia, R.D. Hanson, Influence of ADAS element parameters on building seismic response, *ASCE J. Struct. Eng.* 118 (7) (1992) 1903–1918.
- [14] W.S. Pong, C.S. Tsai, K.C. Tsai, G.C. Lee, Parametric study of TPEA devices for buildings, *Proc. First World Conf on Struct. Cont.*, Los Angeles 1994, pp. 33–42 (1:WP3).
- [15] M. Nakashima, S. Iwai, M. Iwata, T. Takeuchi, S. Konomi, T. Akazawa, K. Saburi, Energy dissipation behaviour of shear panels made of low yield steel, *Earthq. Eng. Struct. Dyn.* 23 (12) (1994) 1299–1313.
- [16] C. Durucan, M. Dicleli, Analytical study on seismic retrofitting of reinforced concrete buildings using steel braces with shear link, *Eng. Struct.* 32 (10) (2010) 2995–3010.
- [17] P. Dusicka, A.M. Itani, I.G. Buckle, Cyclic behavior of shear links of various grades of plate steel, *ASCE J. Struct. Eng.* 136 (4) (2010) 370–378.
- [18] D.C. Rai, B.J. Wallace, Aluminium shear link for enhanced seismic resistance, *Earthq. Eng. Struct. Dyn.* 27 (4) (1998) 315–342.
- [19] S. Jain, D.C. Rai, D.R. Sahoo, Post-yield cyclic buckling criteria for aluminum shear panels, *ASME J. Appl. Mech.* 75 (2) (2008) 1–5 (020105).
- [20] G. De Matteis, F.M. Mazzolani, S. Panico, Experimental tests on pure aluminium shear panels with welded stiffeners, *Eng. Struct.* 30 (6) (2008) 1734–1744.
- [21] G. De Matteis, A. Formisano, S. Panico, F.M. Mazzolani, Numerical and experimental analysis of pure aluminium shear panels with welded stiffeners, *Comput. Struct.* 86 (6) (2008) 545–555.
- [22] G. De Matteis, G. Brando, F.M. Mazzolani, Hysteretic behaviour of bracing-type pure aluminium shear panels by experimental tests, *Earthq. Eng. Struct. Dyn.* 40 (10) (2011) 1143–1162.
- [23] G. De Matteis, G. Brando, F.M. Mazzolani, Pure aluminium: an innovative material for structural applications in seismic engineering, *Constr. Build. Mater.* 26 (1) (2012) 677–686.
- [24] D.C. Rai, P.K. Annam, T. Pradhan, Seismic testing of steel braced frames with aluminium shear yielding dampers, *Eng. Struct.* 46 (6) (2012) 737–747.
- [25] G. de Matteis, A. Formisano, F.M. Mazzolani, An innovative methodology for seismic retrofitting of existing RC buildings by metal shear panels, *Earthq. Eng. Struct. Dyn.* 38 (1) (2008) 61–78.
- [26] D.R. Sahoo, D.C. Rai, A novel technique seismic strengthening of RC frame using steel caging and aluminum shear yielding device, *Earthquake Spectra* 25 (2) (2009) 415–437.
- [27] D.R. Sahoo, D.C. Rai, Seismic strengthening of non-ductile reinforced concrete frames using aluminum shear links as energy-dissipation devices, *Eng. Struct.* 32 (11) (2010) 3548–3557.
- [28] D.R. Sahoo, D.C. Rai, Design and evaluation of seismic strengthening techniques for RC buildings with soft-story, *Eng. Struct.* 56 (11) (2013) 1933–1944.
- [29] R.-W.K. Chan, F. Albermani, Experimental study of steel slit damper for passive energy dissipation, *Eng. Struct.* 30 (2008) 1058–1066.
- [30] K. Ghabraie, R.-W.K. Chan, X. Huang, Y.-M. Xie, Shape optimization of metallic yielding devices for passive mitigation of seismic energy, *Eng. Struct.* 32 (2010) 2258–2267.
- [31] T.L. Karavasilis, S. Kerawala, E. Hale, Hysteretic model for steel energy dissipation devices and evaluation of a minimal-damage seismic design approach for steel buildings, *J. Constr. Steel Res.* 70 (2012) 358–367.
- [32] K. Sugioka, N. Hamada, H. Kobayashi, T. Nishioka, N. Sugiyama, Experimental study on elastoplasticity characteristics of shear panel dampers for long span bridges, *J. Corros. Sci. Eng.* 57A (2011) 528–541.
- [33] S.E. Abdel Raheem, T. Hayashikawa, Energy dissipation system for earthquake protection of cable-stayed bridge towers, *Earthq. Eng. Struct. Dyn.* 5 (6) (2013) 657–678.
- [34] F. Bleich, *Buckling Strength of Metal Structures*, McGraw-Hill, New York, 1952.
- [35] K. Kasai, E.P. Popov, Cyclic web buckling control for shear link beams, *ASCE J. Struct. Eng.* 112 (3) (1986) 505–523.
- [36] FEMA-461, *Interim Testing Protocols for Determining the Seismic Performance Characteristics of Structural and Nonstructural Components*, Federal Emergency Management Agency, Washington, DC, 2007.
- [37] IS:1608, *Indian Standard Mechanical Testing of Metals—Tensile Testing*, Bureau of Indian Standards, New Delhi, 1995.
- [38] FEMA-356, *Prestandard and Commentary for the Seismic Rehabilitation of Buildings*, Federal Emergency Management Agency, Washington, DC, 2000.
- [39] ABAQUS 6.10, Dassault Systèmes Simulia Corporation, Providence, RI, USA; 2011.